Letters

Analysis and Design of Cost-Effective WPT Systems With Dual Independently Regulatable Outputs for Automatic Guided Vehicles

Chenyan Zhu, Jie Yu, Yundong Gu, Jianfeng Gao, Huanyu Yang, Ruikun Mai, *Senior Member, IEEE*, Yong Li, *Member, IEEE*, and Zhengyou He, *Senior Member, IEEE*

***Abstract*—Recently, wireless power transfer (WPT) charging systems have been attracting extensive attention for overcoming the drawbacks of the traditional plugging charging systems, making it a promising candidate for automatic guided vehicles (AGVs). As far as AGVs' applications are concerned, it is quite essential to lower the cost and save space. In order to supply power to both the driving system and control system simultaneously, a dual independently regulatable outputs WPT system without dc–dc converters is presented. Only two diodes and two MOSFETs are employed for the rectifier circuit on the secondary side. A 500-W prototype is built to verify the feasibility of the proposed system. Experimental results show that when a load varies and its output current is regulated with open-loop control, the maximum output current fluctuation of the other load is only $\pm 0.688\%$, and the verified dual outputs are independently regulatable. With closed-loop control, the output voltages can be regulated to the desired ones and remain constant when the loads alter or misalignments happen. The overall efficiency ranges from 86.22% to 90.93%.**

***Index Terms*—Automatic guided vehicles (AGVs), dual independently regulatable outputs (DIRO), wireless power transfer (WPT).**

I. Introduction

In recent years, with the rapid growth of the logistics market and the demand for flexible automation, the number of automatic guided vehicles (AGVs) has significantly increased. In 2019, the sales volume of AGVs in the Chinese market reached up to 6.175 billion RMB. For the plugging charging systems, the AGVs are imposed on traveling the extra distance to the charging stations. Also, queuing time is another drawback when multiple AGVs are waiting to recharge simultaneously. Besides, the connector is prone to damage due to the electrical spark caused by frequently plug-in/plug-out actions, leading to high maintenance costs. The wireless power transfer (WPT) technique is one of the possible solutions for AGVs' charging, as it can overcome the drawbacks mentioned above [1]–[3]. However, since the number of AGVs has grown rapidly, low cost has become one of the most important concerns, and a compact structure is also essential. Hence, the WPT charging system with fewer semiconductor devices and passive components is acclaimed.

For AGVs' charging, there are two independent batteries to supply power for the driving system and control system, respectively. The AGVs have various power ratings, and the charging requirements of two batteries are also different (normally 24 and 48 V for driving system and 12 and 24 V for control system) [4], [5]. Thus, dual outputs with different voltage levels are required. Besides, the requested charging modes of the batteries are unpredictable. Thus, the WPT system is preferred to have dual independently regulatable outputs (DIRO).

The technical schemes to enable the WPT system to realize dual outputs can be roughly classified into two categories: the system with a single transmitter and single receiver, and the system with dual receivers.

First, the general WPT system includes one transmitter and one receiver, which can produce a fixed output when the parameters are determined. In order to provide dual outputs, the method of parallelling the dc-dc converter to the output of the rectifier is presented [6], [7]. Whereas, the extra space is occupied since an additional dc-dc converter is requested. The double T resonant circuit is another feasible approach to provide dual outputs, which achieves voltage conversion by configuring the parameters of the double T resonant circuit [8], [9] at the cost of more passive components and semiconductor devices.

Second, the system with dual transmitter and dual receiver is proposed to achieve two independent power deliveries [10], [11]. However, the cost is relatively high, and the volume is bulky. Thus, in order to reduce the volume, the method of achieving dual outputs by one transmitter and dual receiver is proposed [12]. Nevertheless, the presence of cross-coupling between the receivers induces interference between outputs. Based on the above method, a decoupling circuit employing an additional

Manuscript received July 20, 2020; revised August 23, 2020 and September 30, 2020; accepted October 26, 2020. Date of publication November 6, 2020; date of current version February 5, 2021. This work was supported in part by the National Natural Science Foundation of China under Grants 51677155, 51977184, and 51907169, in part by the Sichuan Youth Science and Technology Innovation Research Team under Grant 2020JDT0004, in part by the Sichuan Science and Technology Program under Grant 2020YFH0031, and in part by the Fundamental Research Funds for the Central Universities under Grant 2682020CX16. *(Corresponding author: Ruikun Mai.)*

The authors are with the Key Laboratory of Magnetic Suspension Technology and Maglev Vehicle, Ministry of Education, Southwest Jiaotong University, Chengdu 611756, China (e-mail: zcy@my.swjtu.edu.cn; yujie1315@126.com; 986663689@qq.com; 1782607776@qq.com; 983911020@qq.com; mairk@swjtu.edu.cn; leeo1864@163.com; hezy@home.swjtu.edu.cn).

Color versions of one or more of the figures in this article are available online at https://ieeexplore.ieee.org.

Digital Object Identifier 10.1109/TPEL.2020.3036353

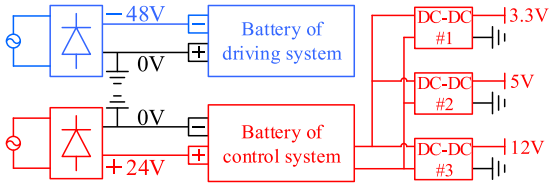

Fig. 1. Configuration for AGVs' batteries.

capacitor to eliminate the influence between receivers without complicated control is proposed [13]. Whereas, the outputs are unable to be independently regulated.

For further deployment of the WPT system for AGVs, the low cost, compact structure, and DIRO are preferred. As for some specifications of AGVs, the batteries share the common ground, and there are several isolated dc-dc converters paralleled to the battery of the control system to realize the voltage conversions of 3.3, 5, and 12 V for the control chips and devices. Then, the devices share the same ground as shown in Fig. 1.

In this letter, the feasibility of adopting two MOSFETs and two diodes on the secondary side to achieve independent regulation for dual outputs is investigated. The proposed DIRO WPT system provides one load with a portion of the charge contained in the secondary current during its positive half cycle, and a portion of the charge contained in the negative half cycle is fed to the other load. By controlling charging durations for each load, their voltages can be independently regulated. Compared with the methods mentioned before, only four power semiconductor devices, a coupler, and corresponding passive components are needed.

II. Proposed DIRO WPT System

A. Circuit Configuration

The proposed DIRO WPT system consists of the primary compensated circuit (L_p and C_p), secondary compensated circuit (L_s and C_s), a bidirectional switch (Q_1 and Q_2), dual outputs half-wave rectifier circuit (D_1, D_2, C_{f1}, C_{f2}, R_1, and R_2), synchronization circuit, and digital signal processor (DSP) as shown in Fig. 2(a). M represents the mutual inductance.

The operating resonant angle frequency of the proposed system is ω. When the bidirectional switch is open, according to Kirchhoff's voltage law, the system can be described as

$$\begin{bmatrix} j\omega L_p + \frac{1}{j\omega C_p} & -j\omega M \\ -j\omega M & j\omega L_s + \frac{1}{j\omega C_s} + R_{\text{ac}} \end{bmatrix} \begin{bmatrix} \dot{I}_p \\ \dot{I}_s \end{bmatrix} = \begin{bmatrix} \dot{V}_p \\ 0 \end{bmatrix} \quad (1)$$

where

$$\omega = 1/\sqrt{L_P C_P} = 1/\sqrt{L_S C_S}. \quad (2)$$

After solving (1), the current of the receiver coil is obtained as

$$\dot{I}_s = j\dot{V}_p/(\omega M). \quad (3)$$

According to the circuitry analysis, the secondary current I_s is independent of the load and only relates to the output of ac voltage source V_p and mutual inductance M, which are considered as fixed in the given AGVs' applications. Thus, the secondary current I_s is constant, and the equivalent circuit of the secondary side can be simplified as shown in Fig. 2(b).

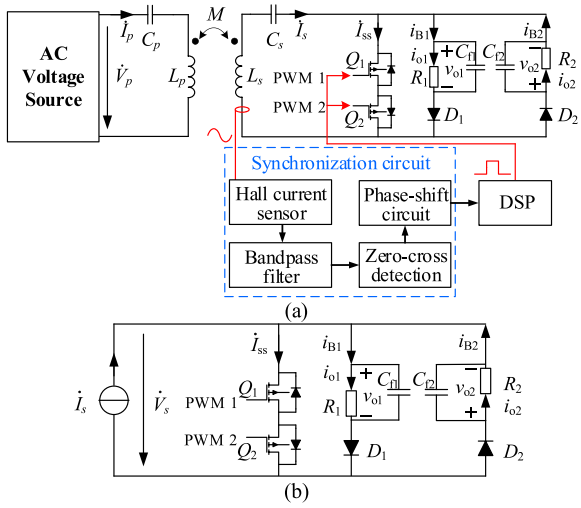

Fig. 2. Schematic diagram of the proposed DIRO WPT system. (a) Composition of the system. (b) Simplified equivalent circuit.

B. Operational Principles

In order to demonstrate the operating principles of the proposed regulatable dual-load WPT system, the adopted assumptions are given as follows.

1) The equivalent resistances of the passive components and parasitic resistances of the diodes and MOSFETs are sufficiently small, which can be neglected.
2) The output capacitors C_{f1} and C_{f2} are relatively large. Thus, the dc outputs are relatively constant.

As shown in Fig. 2(a), the Hall current sensor is employed to detect the secondary current I_s. After passing the bandpass filter, zero-cross detection circuit, and phase-shift circuit, the square wave which has the same frequency and phase angle with I_s is generated and sent to the DSP. Therefore, the required driving signals PWM1 and PWM2 are generated. To simplify the analysis, assume D_{Q1} is the duty cycle of PWM1 in the positive half period and D_{Q2} is the duty cycle of PWM2 in the negative half period. Fig. 3 illustrates the operational principle of the proposed circuit, and there are four modes in total for a working period. The critical waveforms of the proposed DIRO WPT system are depicted in Fig. 4.

Mode 1 [At time $nT_s \sim nT_s + D_{Q1}{\cdot}T_s$]: Mode 1, as depicted in Fig. 3(a), MOSFET Q_1 turned ON in the negative half period and remained in the ON-state. Due to the existence of an antiparallel of MOSFET Q_2, a short circuit branch forms, and the secondary current I_s flows into Branch I. After a short delay, the voltage of MOSFET Q_2 drops to zero, where MOSFET Q_2 turns ON, and zero voltage switch (ZVS) turn-ON is achieved. At this period, the current source does not supply power for loads.

Mode 2 [At time $nT_s + D_{Q1}{\cdot}T_s \sim nT_s + T_s/2$]: Mode 2, as shown in Fig. 3(b), MOSFET Q_2 keeps the ON-state, and MOSFET Q_1 turns OFF at $nT_s + D_{Q1}{\cdot}T_s$. Thereby, since the antiparallel

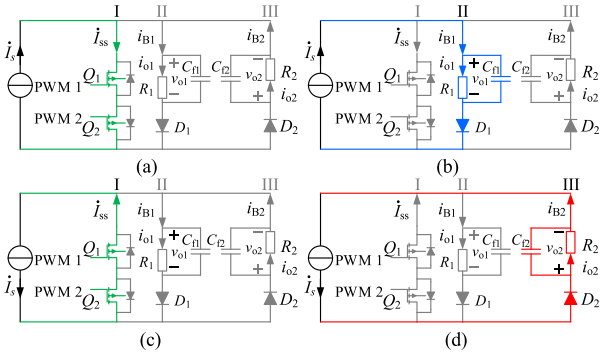

Fig. 3. Equivalent circuit models of four operational modes of the proposed DIRO WPT system.

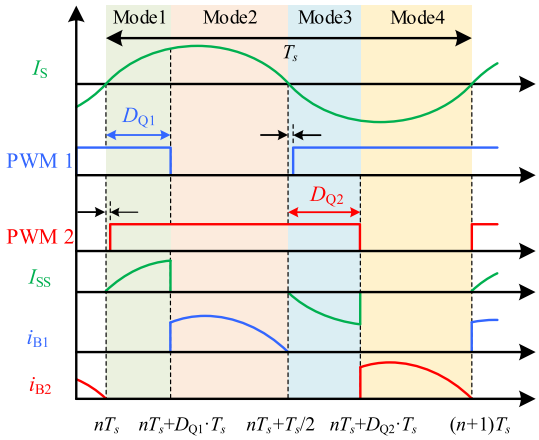

Fig. 4. Key waveforms of the proposed DIRO WPT system.

diode of MOSFET Q_1 blocks the current, the secondary current I_s will no longer flow into Branch I but Branch II and supplies power for load R_1 until $nT_s + T/2$, when the positive half period ends.

Mode 3 [At time $nT_s + T_s/2 \sim nT_s + D_{Q2}{\cdot}T_s$]: Mode 3, the negative half period starts, and the secondary current I_s is opposite. Since MOSFET Q_2 is still in the ON-state, the secondary current I_s will flow into Branch I consisting of MOSFET Q_2 and an antiparallel diode of MOSFET Q_1. Then, MOSFET Q_1 turns ON when its voltage drops to zero, thereby the ZVS turn-ON is achieved, as shown in Fig. 3(c).

Mode 4 [At time $nT_s + D_{Q2}{\cdot}T_s \sim (n+1)T_s$]: Mode 4, MOSFET Q_1 remains in the ON-state, and MOSFET Q_2 turns OFF at $nT_s + D_{Q2}{\cdot}T_s$. Therefore, since the antiparallel diode of MOSFET Q_2 blocks the current, the secondary current I_s flows into Branch III, and load R_2 is supplied until the negative half period ends, as shown in Fig. 3(d).

Thus, the load R_1 (R_2) is powered in the positive half period (negative half period) of the secondary current I_s. The output branch currents i_{B1} (i_{B2}) can be regulated by adjusting the duration of Mode 2 (Mode 4).

By filtering by the capacitors, the currents of loads i_{o1} and i_{o2}, are only the dc components of the branch currents i_{B1} and i_{B2}. Thus, the rms values of i_{o1} and i_{o2} are equal to the average values of i_{B1} and i_{B2}. According to the above operating status,

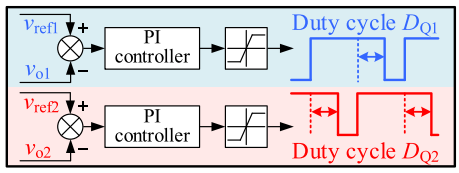

Fig. 5. Block diagram of the controller algorithm.

the rms value of I_s, I_{SS}, i_{o1}, and i_{o2} can be expressed as

$$\begin{cases} I_s = \sqrt{\frac{1}{2\pi}\cdot\int_0^{2\pi}\left(\sqrt{2}I_s\sin(\omega t)\right)^2 d\omega t} = \frac{V_P}{\omega M} \\ I_{SS} = \sqrt{\frac{1}{2\pi}\cdot\left[\int_0^{2\pi\cdot D_{Q1}}\left(\sqrt{2}I_s\sin(\omega t)\right)^2 d\omega t + \int_{\pi}^{\pi+2\pi\cdot D_{Q2}}\left(\sqrt{2}I_s\sin(\omega t)\right)^2 d\omega t\right]} \\ = \frac{V}{2\sqrt{\pi}\omega M}\sqrt{\sin(4\pi D_{Q1})+\sin(4\pi D_{Q2})-4\pi\left(D_{Q1}+D_{Q2}\right)} \\ i_{o1} = \frac{1}{2\pi}\int_{2\pi\cdot D_{Q1}}^{\pi}\sqrt{2}I_s\sin(\omega t)d\omega t = \frac{\sqrt{2}}{\pi}\cdot\frac{V_P}{\omega M}\cos^2(\pi D_{Q1}) \\ i_{o2} = \frac{1}{2\pi}\int_{\pi+2\pi\cdot D_{Q2}}^{2\pi}\sqrt{2}I_s\sin(\omega t)d\omega t = \frac{\sqrt{2}}{\pi}\cdot\frac{V_P}{\omega M}\cos^2(\pi D_{Q2}). \end{cases} \tag{4}$$

The secondary current I_s is constant, according to (4), the output currents i_{o1} and i_{o2} are load-independent, and only relate to the duty cycles D_{Q1} and D_{Q2}, respectively.

Since the energies before and after rectifying are conserved, the equation can be obtained as

$$I_s^2 \cdot R_{\rm ac} = i_{o1}^2 \cdot R_1 + i_{o2}^2 \cdot R_2. \tag{5}$$

Substituting (4) into (5), the $R_{\rm ac}$ can be expressed as

$$R_{\rm ac} = \frac{R_1[3+4\cos(2\pi D_1)+\cos(4\pi D_1)]+R_2[3+4\cos(2\pi D_2)+\cos(4\pi D_2)]}{4\pi^2}. \tag{6}$$

The output voltages v_{o1} and v_{o2} of the load R_1 and R_2 can be described as

$$\begin{cases} v_{o1} = \frac{\sqrt{2}}{\pi}\cdot\frac{V_P R_1}{\omega M}\cos^2(\pi D_{Q1}) \\ v_{o2} = \frac{\sqrt{2}}{\pi}\cdot\frac{V_P R_2}{\omega M}\cos^2(\pi D_{Q2}). \end{cases} \tag{7}$$

According to (7), for the given output of ac voltage source V_p and mutual inductance M, the output voltages v_{o1} and v_{o2} only depend on the corresponding values of loads and duty cycles. In order to output constant voltages, the duty cycles D_{Q1} and D_{Q2} should be regulated as the loads R_1 and R_2 vary. Thus, the PI controller is used to realize closed-loop constant voltage control, as shown in Fig. 5.

III. Experimental Results

In order to verify the feasibility of the proposed DIRO WPT system, a 500 W experimental prototype operating at 85 kHz switching frequency is fabricated, as shown in Fig. 6.

The design flowchart of system parameters is shown in Fig. 7. Since the output of ac voltage source V_p and the operating frequency ω of the proposed system are given, according to the desired output currents i_{o1} and i_{o2} and output voltages v_{o1} and v_{o2}, the mutual inductance M can be calculated by (4). Then, the coupler having desired mutual inductance M will be constructed, and self-inductances and compensation capacitors are determined. The parameters of the proposed system are listed in Table I.

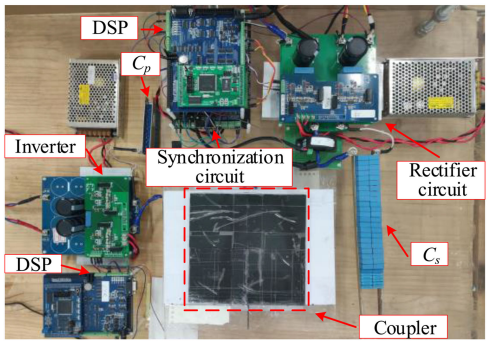

Fig. 6. Prototype of the proposed DIRO WPT system.

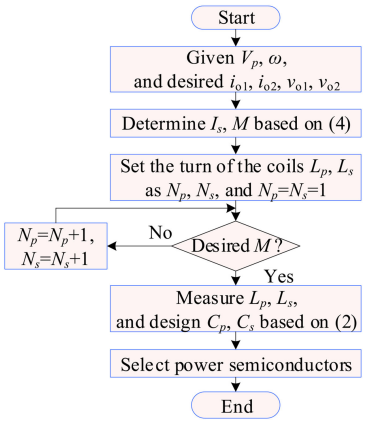

Fig. 7. Implementation chart of the proposed DIRO WPT system.

TABLE I
SYSTEM SPECIFICATION AND PARAMETER VALUES

Parameter	Value	Parameter	Value
V_p	100 V	M	14.425 μH
L_p	63.85 μH	L_s	63.52 μH
C_p	54.70 nF	C_s	55.07 nF

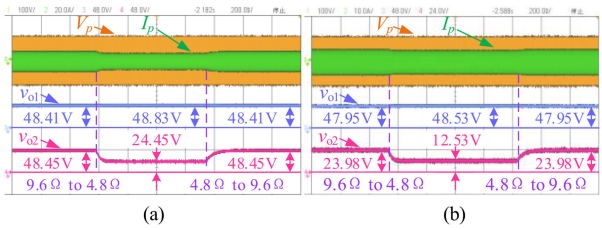

Fig. 8. Experimental waveforms with open-loop control when load R_2 step changes happen. (a) $D_{Q1} = D_{Q2} = 0\%$. (b) $D_{Q1} = 0\%$ and $D_{Q2} = 25\%$.

In order to prove that the dual outputs are independent of each other, the open-loop load step changes with different duty cycles are conducted, as shown in Fig. 8. Fig. 8(a) reveals the variations of the output voltages of two loads when $D_{Q1} = D_{Q2} = 0\%$. The initial values of two loads are both set as 9.6 Ω, then load R_2 alters from 9.6 to 4.8 Ω and back to 9.6 Ω. The output voltage v_{o2} at the first moment varies from 48.45 to 24.45 V and raises back to 48.45 V at the second moment. On the other hand, the output voltage v_{o1} of the two moments are basically the same (48.41 to 48.83 to 48.41 V). Furthermore, the variation of the

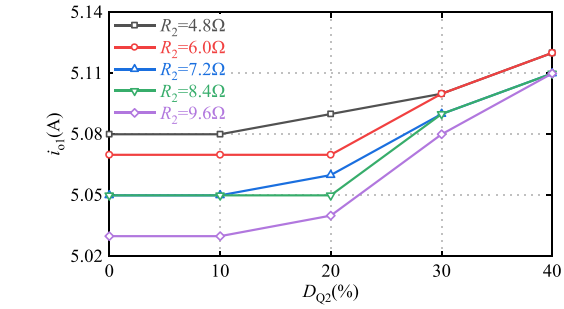

Fig. 9. Measured output current i_{o1} when R_2 and D_{Q2} vary.

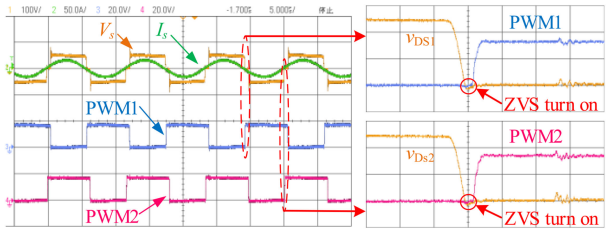

Fig. 10. ZVS turn-ON operations of the MOSFETs.

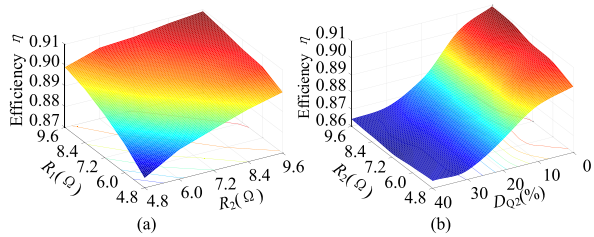

Fig. 11. Experimental efficiencies (a) versus R_1 and R_2 and (b) versus R_2 and D_{Q2}.

output voltages of two loads when $D_{Q1} = 0\%$ and $D_{Q2} = 25\%$ with the same step changes is shown in Fig. 8(b). The output voltage v_{o1} at two moments are with a minor difference (47.95 to 48.53 to 47.95 V), while the output voltage v_{o2} halves and doubles (23.98 to 12.53 to 23.98 V). It is observed that load R_2 changes 100%, but output voltage v_{o1} barely alters and even duty cycles are different. Fig. 9 illustrates the measured output current i_{o1} when the load $R_1 = 9.6$ Ω, while load R_2 alters from 4.8 to 9.6 Ω and D_{Q2} varies from 0% to 40%. The fluctuation of the output current i_{o1} is only within ±0.688%. Therefore, it is verified that the dual outputs are independent of each other, and the system has good load-independent constant current output performance.

Fig. 10 shows the secondary voltage/current and driving signals of MOSFETs when $R_1 = R_2 = 9.6$ Ω, $D_{Q1} = D_{Q2} = 10\%$. It is observed that the ZVS turn-ON operations of MOSFETs are achieved, respectively, to reduce the switching losses. Fig. 11(a) shows experimental efficiencies when the two loads vary from 4.8 to 9.6 Ω, respectively, which ranges from 87.48% to 90.93%. And the corresponding efficiencies are measured when load R_1 = 9.6 Ω and load R_2 alters from 4.8 to 9.6 Ω with variational duty cycles, as shown in Fig. 11(b). The overall efficiency ranges from 86.22% to 90.93%.

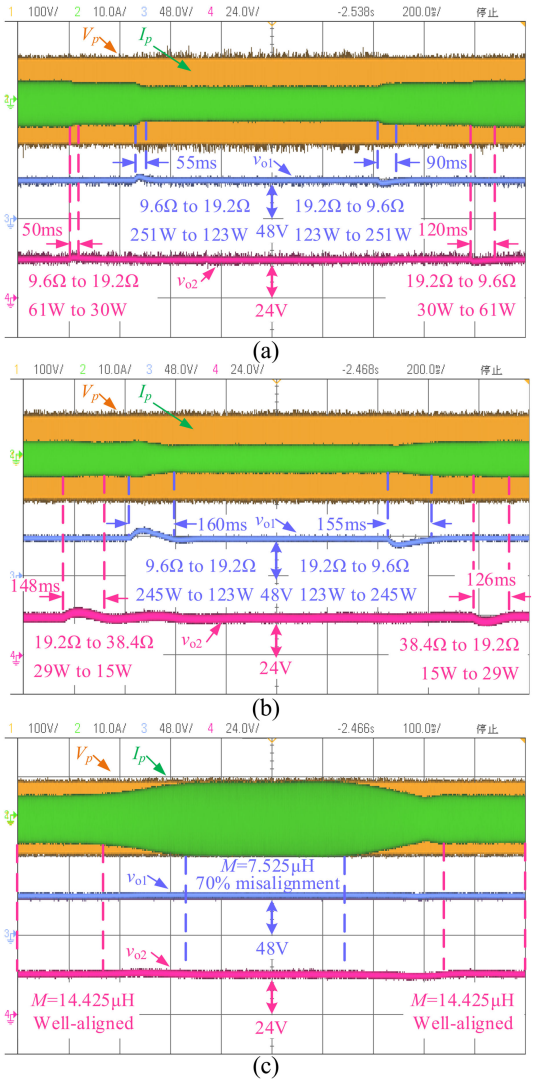

Fig. 12. Dynamic responses with closed-loop constant voltage control under (a) balanced loads conditions with rated voltages, (b) unbalanced loads conditions with rated voltages, and (c) sudden misalignment conditions.

Fig. 12 illustrates the dynamic responses with closed-loop voltage control. Fig. 12(a) reveals variations of the output voltages under balanced loads conditions with rated voltages, v_{o1} is set as 48 V and v_{o2} is set as 24 V. The loads R_1 and R_2 alter from 9.6 to 19.2 Ω, then back to 9.6 Ω, and the output voltages v_{o1} and v_{o2} can restore to the rated voltage within 120 ms. Fig. 12(b) shows variations of the output voltages under unbalanced load conditions with rated voltages. The load R_1 varies from 9.6 to 19.2 Ω, then back to 9.6 Ω, and R_2 changes from 19.2 to 38.4 Ω, then back to 19.2 Ω. The output voltages v_{o1} and v_{o2} hardly change, and response times are 160 ms. Moreover, the experiment under sudden misalignment conditions is conducted when $R_1 = R_2 = 9.6\ \Omega$, $v_{o1} = 48$ V, and $v_{o2} = 24$ V. The mutual inductance M changes from 14.425 to 7.425 μH and back to 14.425 μH (70% misalignment), and the output voltages hardly vary, as shown in Fig. 12(c). Therefore, the experimental results illustrate that the dual outputs are both able to resist load step changes effectively under load balance/unbalance conditions and keep stable when sudden misalignments happen.

IV. Conclusion

In this article, a DIRO WPT system is proposed for charging the driving system and control system of AGVs, simultaneously. Compared with the methods mentioned above to realize dual outputs, the proposed WPT system only requires four power semiconductor devices, a coupler, and corresponding passive components without additional dc-dc converter, and the dual outputs can be regulated independently. The experimental results validate that outputs are independent of each other. The fluctuation of the output current i_{o1} is within $\pm 0.688\%$ when the load $R_1 = 9.6\ \Omega$ while R_2 changes from 4.8 to 9.6 Ω and D_{Q2} varies from 0% to 40%. Also, the proposed WPT system can achieve output regulation by controlling the duty cycles of the driving signals. The overall efficiency ranges from 86.22% to 90.93%. Besides, the dual outputs are both able to resist load step changes effectively and sudden misalignments with closed-loop voltage control. Future work may consider using fewer semiconductor devices and improve efficiency.

References

[1] Y. Li *et al.*, "A new coil structure and its optimization design with constant output voltage and constant output current for electric vehicle dynamic wireless charging," *IEEE Trans. Ind. Informat.*, vol. 15, no. 9, pp. 5244–5256, Sep. 2019.

[2] Y. Li *et al.*, "Analysis, design, and experimental verification of a mixed high-order compensations-based WPT system with constant current outputs for driving multistring LEDs," *IEEE Trans. Ind. Electron.*, vol. 67, no. 1, pp. 203–213, Jan. 2020.

[3] B. Luo, A. P. Hu, H. Munir, Q. Zhu, R. Mai, and Z. He, "Compensation network design of CPT systems for achieving maximum power transfer under coupling voltage constraints," *IEEE J. Emerg. Sel. Top. Power Electron.*, early access, doi: 10.1109/JESTPE.2020.3027348.

[4] F. Lu *et al.*, "A tightly coupled inductive power transfer system for low-voltage and high-current charging of automatic guided vehicles," *IEEE Trans. Ind. Electron.*, vol. 66, no. 9, pp. 6867–6875, Sep. 2019.

[5] "LD-Series-Mobile-Robot-Datasheet." [Online]. Available: https://assets.omron.com/m/1bf71ca06f961b4b/original/LD-Series-Mobile-Robot-Datasheet.pdf

[6] J. Hu *et al.*, "Hybrid energy storage system of an electric scooter based on wireless power transfer," *IEEE Trans. Ind. Informat.*, vol. 14, no. 9, pp. 4169–4178, Sep. 2018.

[7] M. McDonough, "Integration of inductively coupled power transfer and hybrid energy storage system: A multiport power electronics interface for battery-powered electric vehicles," *IEEE Trans. Power Electron.*, vol. 30, no. 11, pp. 6423–6433, Nov. 2015.

[8] Y. Li, J. Hu, X. Li, and K. E. Cheng, "A flexible load-independent multi-output wireless power transfer system based on cascaded double t-resonant circuits: Analysis, design and experimental verification," *IEEE Trans. Circuits Syst. I: Regular Papers*, vol. 66, no. 7, pp. 2803–2812, Jul. 2019.

[9] Y. Li *et al.*, "Analysis, design, and experimental verification of a mixed high-order compensations-based wpt system with constant current outputs for driving multistring LEDs," *IEEE Trans. Ind. Electron.*, vol. 67, no. 1, pp. 203–213, Jan. 2020.

[10] B. L. Cannon, J. F. Hoburg, D. D. Stancil, and S. C. Goldstein, "Magnetic resonant coupling as a potential means for wireless power transfer to multiple small receivers," *IEEE Trans. Power Electron.*, vol. 24, no. 7, pp. 1819–1825, Jul. 2009.

[11] D. Ahn and S. Hong, "Effect of coupling between multiple transmitters or multiple receivers on wireless power transfer," *IEEE Trans. Ind. Electron.*, vol. 60, no. 7, pp. 2602–2613, Jul. 2013.

[12] L. Sun, H. Tang, and S. Zhong, "Load-independent output voltage analysis of multiple-receiver wireless power transfer system," *IEEE Antennas Wireless Propag. Lett.*, vol. 15, pp. 1238–1241, 2016.

[13] R. Mai, Y. Luo, B. Yang, Y. Song, S. Liu, and Z. He, "Decoupling circuit for automated guided vehicles IPT charging systems with dual receivers," *IEEE Trans. Power Electron.*, vol. 35, no. 7, pp. 6652–6657, Jul. 2020.